Self-consistent 2-D numerical modeling and simulation of a uniformly doped nanoscale double-gate SOI n-MOSFET under illuminated condition for photodetection application

M. KABEER[*], V. RAJAMANI[a], S. BOSE[b]
[*]*Department of Information Technology, B. S. AbdurRahman Crescent Engineering College, Chennai, Tamilnadu, India – 600 048*
[a]*Department of Electronics and Communication Engineering, Veltech Multitech Dr.Rangarajan Dr.Sakunthala Engineering College, Avadi, Chennai, Tamilnadu, India – 600 062*
[b]*Department of Computer Science and Engineering, Anna University, Chennai, Tamilnadu, India – 600 025*

A two-dimensional numerical modeling of a uniformly doped nanoscale Double-Gate SOI n-MOSFET under illuminated condition including quantum mechanical effects has been developed. A self-consistent solution of 2-D Poisson-Schrödinger equation has been obtained. Finite differential method is used in solving the Schrödinger equation using mode space approach due to which size of the problem is reduced and sufficient accuracy is obtained. Leibmann's iteration method is used in solving Poisson equation with proper boundary conditions. The exact potential profile of the device under illuminated condition has been computed numerically. The electric field profile along the length and width of the channel and mobility of the carriers have also been studied extensively under illuminated condition to have an in depth analysis. Calculations are being carried out to examine the effect of illumination on the current-voltage characteristics, conduction band vs sub-band energy profile and sub-band electron density. The accuracy of the model has been verified by comparing the results with that calculated by nanomos 2.5 device simulator. Due to effect of photo generation, the device characteristics are strongly influenced. The proposed model is fairly accurate and can be used for accurate simulation of Opto Electronic Integrated Circuits (OEIC) using uniformly doped DG SOI n-MOSFET Photo detector.

(Received November 10, 2012; accepted March 13, 2014)

Keywords: Nanoscale Double Gate SOI n-MOSFET, 2-D Poisson-Schrödinger, Finite differential method, Quantum mechanical effects, Photodetector

1. Introduction

The photosensitivity and integrated circuit compatibility of Field-Effect Transistors (FETs) have extended the potential of these devices for their use as photodetectors. Among the FETs configuration, Metal Semi- conductor Field Effect Transistor (MESFET) and High Electron Mobility Transistor (HEMT) have been studied theoretically as well as experimentally by several researchers for various optically-controlled applications [1-5]. A three dimensional modeling of analog MISFET photodetector without including quantum mechanical effects [6] has been reported.

According to Moore's law, the dimensions of individual devices in an integrated circuit have been decreased by a factor of approximately two every two years. This scaling down of devices has been the driving force in technological advances since late 20th century. However, as noted by ITRS 2009 edition, further scaling down has faced serious limits related to fabrication technology and device performances as the critical dimension shrunk down to sub-22 nm range [7]. CMOS designs below 0.1 μm are severely constrained by short channel effects (SCE) and gate insulator tunneling [8-11]. The limits involve electron tunneling through short channels and thin insulator films, the associated leakage currents, passive power dissipation, short channel effects, and variations in device structure and doping. Today most widely applied device for integrated circuits is the bulk metal-oxide-silicon field-effect-transistor. Double-gate MOSFETs (DGFET) is one of the most promising devices for channel length in the range 10 to30nm [12-15].A transition from bulk to multiple- gate fully depleted (FD) silicon-on-insulator (SOI) offers drive current and better short-channel immunity [16].

SOI devices can operate in partial depletion (PD) or full depletion (FD) mode, depending on the channel silicon film thickness, channel doping concentration and applied biases. Fully-Depleted (FD) silicon-on-insulator (SOI) technology is a promising option for implementing high speed radio-frequency (RF) integrated circuits. Although SOI technology is now being widely used, there still exists the need to develop numerical device models for SOI-based MOSFETs suitable for circuit simulation. The analytical and numerical modeling of the threshold voltage of FD SOI MOSFETs without considering the

quantum mechanical effects has already been reported by numerous authors [17 -31].

Quantum effects gradually dominating electronic transport properties impose severe challenges for device modeling. Numerical simulation with considering quantum effects is today a fundamental approach for exploring characteristics of emerging nano-scale semiconductor structures and devices. Consequently, a computationally efficient numerical scheme is of considerable interest because of the increased numerical complexity.

In device simulations, one is faced with a self-consistent calculation between Schrodinger and Poisson equations. The carrier density is obtained from the transport equation for a given potential, but this potential also depends on the carrier density through the Poisson equation. Owing to a strong non-linear coupling between these two equations, attention must be paid to numerical schemes in order to achieve convergent solutions. Various iteration schemes have been adopted in this field, such as the perturbation method [32], the adaptive heuristic relaxation method [33], the predictor-corrector method [34], etc. Owing to its fast convergence speed, the predictor-corrector method is widely used in two- and three-dimensional quantum simulation for various semiconductor devices [35], such as bulk MOSFET [36], FinFET[37], nanowire transistor [38], cylindrical surrounding gate MOSFETs [39], etc.

In this paper, a self-consistent solution for 2D numerical model of nanoscale Double Gate SOI MOSFET photodetector using finite differential method for the solution of Schrodinger equation and the Leibmann's iteration method to solve the Poisson equation has been developed and presented. The prime focus is to obtain the device characteristics under illumination, by numerically solving the 2D Poisson-Schrodinger equations directly until self-consistency is achieved.

2. Physics based modeling and approach

The general Double Gate Silicon On Insulator MOSFET structure is shown in Fig. 1.

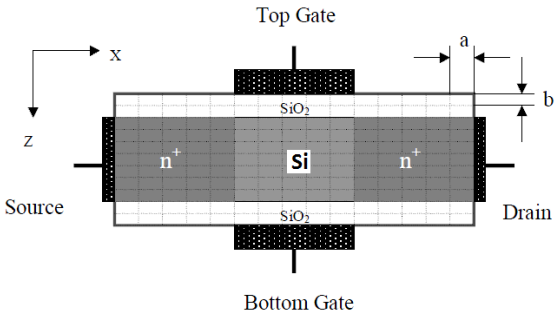

Fig. 1. A Ultra-thin body Double Gate SOI-MOSFET structure.

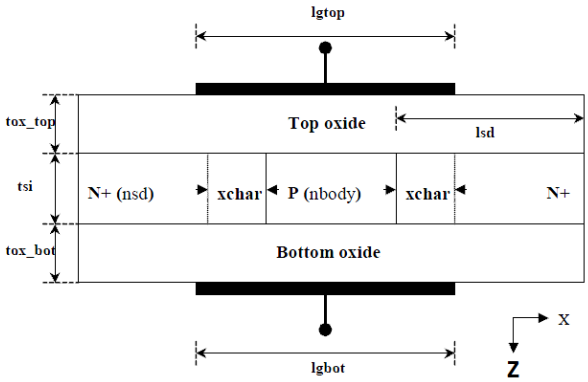

Fig. 2. Parameters to specify the device structure.

The geometrical parameters of the device shown in Fig. 2 is tabulated in Table 1.

Table 1. Geometrical Parameters of the DG SOI-MOSFET.

nsd	Source/Drain doping concentration	10^{20} cm^{-3}
nbody	Body doping concentration (cm-3)	undoped
lgtop	Length of the top gate (nm)	10 nm
lgbot	Length of the bottom gate (nm)	10 nm
lsd	Length of the Source/Drain (nm)	7.5 nm
overlap_s	Source extension length (nm)	0 nm
overlap_d	Drain extension length (nm)	0 nm
tox_top	Top insulator thickness (nm)	1.5 nm
tox_bot	Bottom insulator thickness (nm)	1.5 nm
tsi	Silicon film thickness (nm)	1.5 nm
temp	Lattice temperature (K)	300 K

The above mentioned nanoscale DG SOI MOSFET device is described electrically on quantum mechanical level by two main equations: the first is Poisson equation:

$$\nabla^2 V = -\frac{q}{\varepsilon}\,(p - n + N_D - N_A \qquad (1)$$

From which the electrical potential V can be determined given the quantities in the right hand side including hole and electron distributions p and n, and doping concentrations for donors and acceptors N_D and N_A respectively. In (1) q is electronic charge, and ε is the permittivity of the medium. As we have considered the Double Gate SOI MOSFET, where hole concentration is neglected.

The second equation is Schrodinger equation with effective mass approximation,

$$\frac{-\hbar^2}{2m^*}\nabla^2\Psi - (qV + E)\,\Psi = 0 \qquad (2)$$

which, given the electric potential V, determines Eigen energies E and Eigen functions Ψ from which the electron concentration can be obtained. In (2), $\hbar$ is Planck's constant and m^* is the effective mass of electrons. The transport of carriers in nanoscale DG devices is nearly ballistic [40], so, no scattering are included in the solution of (2). Equations (1) and (2) are coupled such that the solution of any one requires the result of the other; consequently, they are solved by iterative method until self-consistence is obtained. The methods used for solving the 2D Poisson Equation (1) and the Schrodinger equation (2) are discussed in the following sections.

2.1. Solving Schrödinger equation

The Schrödinger is discretized using the mode-space representation approach. This approach greatly reduces the size of the problem and provides sufficient accuracy when compared to full 2D spatial discretization [41]. Referring to Fig. 1, a double-gate SOI device is divided into vertical slices, each of width 'a'. For each vertical slice at x = x`, an 1D effective mass equation in the z direction is written as

$$\frac{-\hbar^2}{2m_z^*}\frac{d^2\Psi(x',z)}{dz^2} + (U(x',z) - E)\Psi(x',z) = 0 \qquad (3)$$

Where m_z^* is the effective mass of electrons in the z-direction and U= -qV is the potential energy. This equation is solved subject to zero boundary conditions at both upper and lower interfaces assuming nearly infinite conduction band offset between Si and SiO_2, (nearly infinite potential barriers imposed by upper and lower oxides means zero Eigen function there) to obtain a discrete set of Eigen energies and corresponding Eigen functions, i.e., a set of modes. For each mode 'm', the distribution of Eigen energies $E_m(x)$ along the *x*-direction resulting from the solution of Eqn.(3) is used to solve the lD Schrodinger equation in the x-direction,

$$\frac{-\hbar^2}{2m_x^*}\frac{d^2\varphi^{(m)}(x)}{dx^2} - (E - E_m(x))\varphi^{(m)}(x) = 0 \qquad (4)$$

Subject to open boundary conditions at source (left boundary) and drain(right boundary), where m_x^* is the effective mass of electrons in the x-direction. Eqn.(4) is solved twice, one assuming a plane wave is incident from the source contact, in which the solution is termed $\varphi_s^{(m)}$, and the other assuming a plane wave is incident from the drain contact, where the solution is termed $\varphi_D^{(m)}$.The m-mode contribution to the total electron density is thus found from [42],

$$n^{(m)} = \frac{1}{\hbar a}\sqrt{\frac{m_z^* K_B T}{2\pi^3}}\int_{-\infty}^{+\infty}\left[\Im_{-1/2}(F_s - E|\varphi_s^{(m)}(x)|^2 + \Im_{-1/2}(F_D - E|\varphi_D^{(m)}(x)|^2\right]dE \qquad (5)$$

where, $\hbar$ is the modified Planck's constant, m_z^* is the effective mass of electrons in the z-direction, K_B is the Boltzmann constant, T is temperature, $\Im_{-1/2}$ is the Fermi-Dirac integral of order -1/2 [43], F_s and F_D are the Fermi levels at source and drain contacts respectively.

The total electron density within the device is found by the sum of all contributions of individual modes weighted by the probability function $|\Psi_m(x, z)|^2$ of each mode resulting from the solution of Eqn.(3), i.e.,

$$n(x,z) = \sum_m n^{(m)}|\Psi_m(x, z)|^2 \qquad (6)$$

From a computational point of view, if we have N_z points in the z-direction and N_x points in the x-direction, the full 2D discretization will lead to $N_z X\ N_x$ points and this requires the solution of $N_z N_x$ x $N_z N_x$ matrices. On the other hand, using the above mode-space approach, we solve N_z x N_z matrices in the z-direction to find modes, then, we solve N_x x N_x matrices in the x

direction for each mode. The number of operations in mode space is on the order of N_x x (N_z x N_z) +N_m x (N_x x N_x), where N_m is the number of modes. Therefore, if only the first few modes are taken into account, the latter approach provides enormous savings in the computational burden [44].

For the solution of Eqns. (3) and (4) Finite Difference Method (FDM) is used. In this method, the domain of solution is divided into small intervals and a certain approximation, as explained hereinafter, is made within each interval such that the differential equation is transformed to a system of equations which solved to yield the Eigen energies and the distribution of the wave function. The application of the FDM for the solution of Schrödinger equation within double-gate SOI MOSFET is explained in the following section.

2.2. Finite difference method

The FDM subdivides the simulation domain into small discrete segments separated by N nodal points in the transverse direction of the device DG SOI MOSFET as shown in the Fig. 3. The method is based on defining unknown variable only on these nodal points assuming linear variation in between. The derivatives in the differential equation to be solved are thus replaced by discretized finite-difference approximations at each one of the nodes.

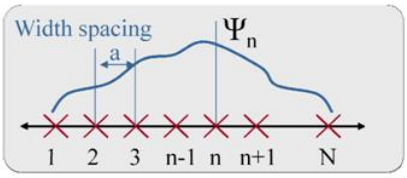

Fig. 3. Discretization of simulation domain of DG SOI n-MOSFET into N nodal points in the transverse direction.

At each particular point, the schrodinger Eqn.(3) can be written as (dropping the value for U)

$$E\Psi_{\mathrm{n}} = \frac{\hbar^2}{2m_z^*}\left(\frac{d^2\Psi}{dz^2}\right)_{\mathrm{n}} \tag{7}$$

where, $$\left(\frac{d^2\Psi}{dz^2}\right)_n = \frac{\left(\frac{d\Psi}{dz}\right)_{\mathrm{n+1/2}} - \left(\frac{d\Psi}{dz}\right)_{\mathrm{n\text{-}1/2}}}{a} \tag{8}$$

where $$\left(\frac{d\Psi}{dz}\right)_{\mathrm{n+1/2}} = \frac{\Psi_{\mathrm{n+1}} - \Psi_{\mathrm{n}}}{a}$$ and

$$\left(\frac{d\Psi}{dz}\right)_{\mathrm{n\text{-}1/2}} = \frac{\Psi_{\mathrm{n}} - \Psi_{\mathrm{n\text{-}1}}}{a} \tag{9}$$

Substituting (9) in (8)

$$\left(\frac{d^2\Psi}{dz^2}\right)_n = \frac{\Psi_{\mathrm{n+1}} - 2\Psi_{\mathrm{n}} + \Psi_{\mathrm{n\text{-}1}}}{a^2} \tag{10}$$

Substituting (10) in (7)

$$E\Psi_{\mathrm{n}} = -t_0\left[\Psi_{\mathrm{n+1}} - 2\Psi_{\mathrm{n}} + \Psi_{\mathrm{n\text{-}1}}\right] \tag{11}$$

where $$t_0 = \frac{-\hbar^2}{2m_z^* a^2} \tag{12}$$

Applying equation (11) in the I D Schrodinger equation given in (3), we get.

$$-t_0\left[\Psi_{\mathrm{n+1}} - 2\Psi_{\mathrm{n}} + \Psi_{\mathrm{n\text{-}1}}\right] + \mathrm{U_n}\Psi_{\mathrm{n}} = \mathrm{E}\Psi_{\mathrm{n}} \tag{13}$$

Eqn. (13) is a compact representation of N-2 equations at N-2 interior points. The two points at the boundaries needs special treatment. At the left boundary (point 1) equation (13) becomes

$$-t_0[\Psi_2 - 2\Psi_1 + \Psi_0] + \mathrm{U_1}\Psi_1 = E\Psi_1 \tag{14}$$

And, at the right boundary (point N), becomes,

$$-t_0\left[\Psi_{\mathrm{N+1}} - 2\Psi_{\mathrm{N}} + \Psi_{\mathrm{N\text{-}1}}\right] + \mathrm{U_N}\Psi_{\mathrm{N}} = E\Psi_{\mathrm{N}} \tag{15}$$

In (14) and (15), Ψ_0 and Ψ_{N+1} are the wave functions at the hypothetical points 0 and N+l outside the simulation domain and should be determined from the boundary conditions. For example, in the transverse direction of double-gate SOI MOSFET, the domain is surrounded by infinite potential barriers of zero wave function, thus:

$$\Psi_0 = \Psi_{\mathrm{N+1}} = 0 \tag{16}$$

The complete set of equations (13)- (l5) with the condition (16) is cast in matrix form as,

$$E\begin{bmatrix}\Psi_1\\ \Psi_2\\ \vdots\\ \Psi_n\\ \vdots\\ \Psi_N\end{bmatrix} = \begin{bmatrix}2t_0+U(x_1) & -t_0 & 0 & 0 & 0 & 0\\ -t_0 & 2t_0+U(x_2) & -t_0 & 0 & 0 & 0\\ 0 & -t_0 & \ddots & \ddots & 0 & 0\\ 0 & 0 & \ddots & \ddots & \ddots & 0\\ 0 & 0 & 0 & \ddots & \ddots & -t_0\\ 0 & 0 & 0 & 0 & -t_0 & 2t_0+U(x_N)\end{bmatrix}\begin{bmatrix}\Psi_1\\ \Psi_2\\ \vdots\\ \Psi_n\\ \vdots\\ \Psi_N\end{bmatrix} \tag{17}$$

This Eigen value equation is solved for N different modes. Each mode has an Eigen energy $E^{(m)}$, and corresponding Eigen function values, $\Psi_1^{(m)}, \cdots \Psi_N^{(m)}$ at the N nodal points.

2.3. Solving poisson equation

In order to analyze the DG SOI MOSFET structure under illuminated condition, we need to solve both Poisson's equation and current continuity equation. However, in the sub threshold regime, the currents are small and Poisson's equation alone is sufficient. The 2-D Poisson's equation in the SOI film region is given by,

$$\frac{\partial^2 V}{\partial x^2} + \frac{\partial^2 V}{\partial z^2} = -\frac{q}{\epsilon_{\mathrm{s}}}\left[Na(\mathrm{z}) + \mathrm{p} - \mathrm{n} + \Delta_{\mathrm{n}}\right] \tag{18}$$

where, V is the 2D potential distribution, $N_a(z)$ is the uniform channel doping concentration. n is the electron concentration, p is the hole concentration, q is the electronic charge, and $\epsilon_s$is the permittivity of silicon, Δ_n is the excess carriers generated per unit volume due to illumination, where Δ_n is given by

$$\Delta_{\mathrm{n}} = \frac{1}{W_{\mathrm{m}}}\int_0^{W_{\mathrm{m}}} G_{\mathrm{op}}(x)\,\tau_{\mathrm{L}}\,dy \tag{19}$$

where, W_m is the maximum width of the depletion layer and given by

$$W_{\mathrm{m}} = \left[4\epsilon_{\mathrm{s}}\ln(N_{\mathrm{a}}/n_{\mathrm{i}})/\,q\beta\,N_{\mathrm{a}}\right]^{1/2} \tag{20}$$

where, $G_{op}(x)$ is the excess carrier generation rate at any point *x* in the semiconductor and is given by

$$G_{op}(x) = \frac{p_{opt}}{h\gamma}(1-R_m)(1-R_i)(1-R_s)\alpha e^{-\alpha y} \quad (21)$$

Where, P_{opt} is the incident optical power density, and h is the Planck's constant, γ is the operating frequency, αis the absorption coefficient of the semiconductor at the operating wavelength and Rm, Ri and Rs are the reflection coefficient at the gate entrance, gate-insulator interface and insulator-semiconductor interface respectively.

We are making some assumptions in the above equation. The first assumption used is that hole concentration is negligible for n-MOSFETs. Moreover, for better convergence of the self-consistent loop, *n*(*x*,*z*) is replaced by a new variable, namely, the quasi-fermi potential energy for electrons F_n defined by [44]

$$n = N_c \Im_{1/2}\left[\frac{F_n + qV}{K_n T}\right] \quad (22)$$

Where, N_c is normalization factor, and $\Im_{1/2}$ is the Fermi-Dirac integral of order 1/2 [43] which is an integral of an exponential function of x. The advantage of introducing this variable change is that overestimates in V will increase 'n' through (22) which leads to the decrease of V during the solution of Poisson equation. The basic model equation (18) has been solved numerically using Liebmann's iteration method. The channel profile has been obtained by dividing the channel region into several meshes and the potential distributions have been obtained using the appropriate boundary condition. The length of the channel is divided into equal meshes 'm_x' in longitudinal direction and 'm_z' in the transverses direction.

The boundary conditions used are

$$V(x,z)\big|_{x=0} = V_{bi} + V_{op} \quad (23)$$

$$V(x,z)\big|_{x=Leff} = V_{bi} + V_{ds} + V_{op} \quad (24)$$

$$V(x,z)\big|_{y=0} = V_{gt} - V_{fb}^{\ t} \quad (25)$$

$$V(x,z)\big|_{y=d} = V_{gb} - V_{fb}^{\ b} \quad (26)$$

Where,V_{gt} is top gate volage, V_{gb} is bottom gate voltage, V_{bi} is built in potential in between source/drain and SOI interface, V_{ds} is source to drain voltage, $V_{fb}^{\ t}$is flat band voltage at top gate,$V_{fb}^{\ b}$ is flat band voltage at bottom gate and V_{op} is photovoltage due to illumination which is given by

$$V_{op} = \frac{nKT}{q}\ln\left[\frac{q}{J_{sc}}\,\alpha\,\frac{P_{opt}}{h\gamma L}\left(\int_0^L \int_0^{z_{dg}(x)} \exp(\alpha z)\,dz\,dx\right)\right] \quad (27)$$

where, n is ideality factor, k is Boltzmann constant, T is absolute temperature, z is width of the gate, L is channel length, J_{sc} is reverse saturation current density, $z_{dg}(x)$ is depletion width at x, P_{opt} isincident optical power density, h is Planck's constant, γ is frequency of the incident radiation and α is optical absorption coefficient of the semiconductor at the operating wavelength.

The electric fields along the x and y direction have been obtained from the two dimensional potential distribution in the channel by solving equations

$$E_x = \frac{V(i+1,j) - V(i-1,j)}{2L/m_x} \quad (28)$$

$$E_z = \frac{V(i,j+1) - V(i,j-1)}{2W/m_z} \quad (29)$$

These equations have been utilized for estimating the field dependent mobility and the drain current characteristics. The field dependent mobility have been obtained from

$$\mu_x = \xi_s \xi_r E_x \quad (30)$$

$$\mu_y = \xi_s \xi_r E_z \quad (31)$$

The drain current I_{ds} has been calculated by numerically integrating the charge in the channel region, given by

$$I_{ds} = \frac{z}{L}\int_0^{V_{ds}} \mu_n(E_x, E_z) Q_n(V)\,dv \quad (32)$$

The charge in the neutral channel region $Q_n(V)$ has been computed by,

$$Q_n(V) = q\int_{y_{dg}}^{a} N_d(x,z)\,dy + q\frac{p_{opt}(1-R_m)(1-R_s)\,\alpha\,\alpha_L}{h\nu}\int_0^a \exp(-\alpha z)\,dz \quad (33)$$

where, $\mu_n(E_x,E_z)$ is the field dependent mobility of electrons, $Q_n(V)$ is the charge in the neutral channel region, z is the device width, E_x and E_y are the electric fields in x (horizontal) and z (vertical) directions respectively, y_{dg} is the variation of depletion depth and function of potential distribution in the channel.

3. Computational technique

The flow chart of the computational technique adapted in this numerical modeling and simulation is shown in Fig. 4.

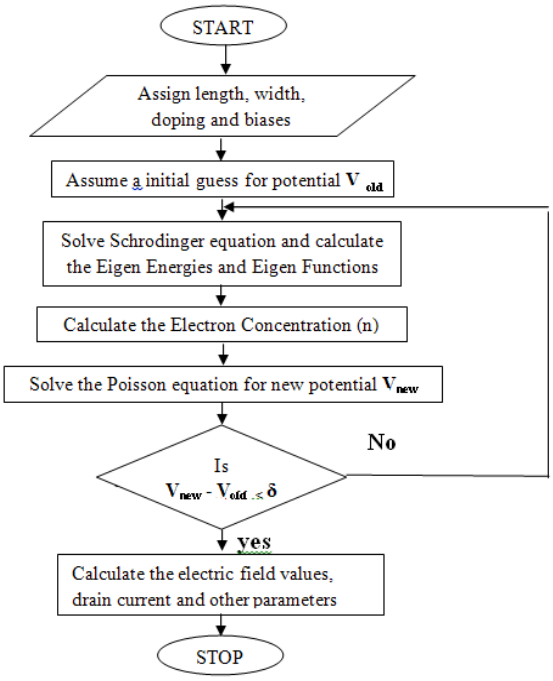

Fig. 4. Flow chart for numerical simulation of DG SOI n-MOSFET.

A rough initial guess for the potential distribution in the device is firstly assumed. According to this potential, Schrodinger equation is solved using Finite Difference Method as discussed in the section 2.2. The Eigen Energies and Eigen functions resulting from the solution of Schrodinger equation are used to calculate the electron concentration in the device. Now, with the electron concentration is known, 2-D Poisson equation is solved using Leibmann's iteration method which yields a new potential distribution. The new potential is compared to the old potential and the solution cycle is repeated until self-consistent solution for the potential is obtained (until the difference in potential between two successive iterations is below a certain tolerance, **δ**).

4. Results and discussion

A fully depleted double-gate SOI n-MOSFET device with n+ source/drain donor doping of 10^{20} cm^{-3} is considered. Both of the top and bottom gate contact work functions are taken to be 4.25 eV. The top and bottom insulator relative dielectric constant is assumed to be 3.9, while that of Si is 11.7. The length of the gate is 10 nm. All simulations are performed at room temperature (T = 300 K). The results are compared with that calculated by nanomos 2.5 [46] which is a device simulator for double-gate SOI n-MOSFETs developed at Purdue university. Nanomos uses FDM for the solution of both Poisson and Schrodinger equations and can solve by either of five transport models. The quantum ballistic model of nanomos is adapted for extracting results used for comparison.

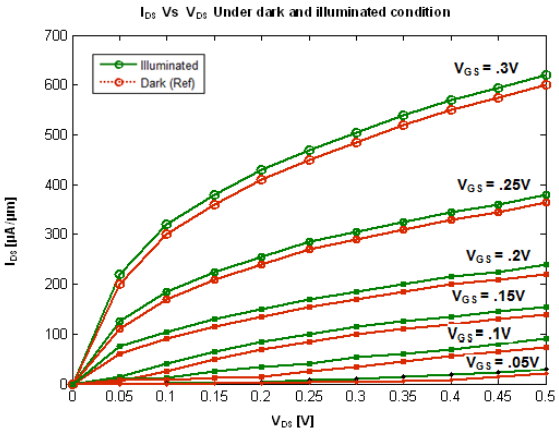

Fig. 5. Simulated I_{DS} versus V_{DS} Characteristics under dark and illuminated conditionsfor various values of V_{GS} ranging from .05 volts to .3 volts.

Fig. 5 shows the comparison of I_{DS} versus V_{DS} (Drain current vs Drain voltage) characteristics of nanoscale n-SOI MOSFET. The values obtained show good agreement with the experimental values. It is also found that the sub-threshold leakage current is well suppressed in spite low channel doping concentration. Also, there seems to be no kink effect, which comes from the effect of a floating body. It is shown that for the applied gate to-source voltage, the drain current also significantly increases. The channel width is determined by applied gate-to-source voltages. The charge carriers pass through the channel and hence the conduction takes place. When the drain voltage is further increased, more charge carriers try to pass through the channel, resulting in an increase in drain current. But these charge carriers passes through the channel width that is created earlier. Hence, the drain current saturates after a certain limit even if the drain voltage is increased further. It is also found that the drain current under illuminated condition is more than under dark condition due to generation of excess carriers under illumination.

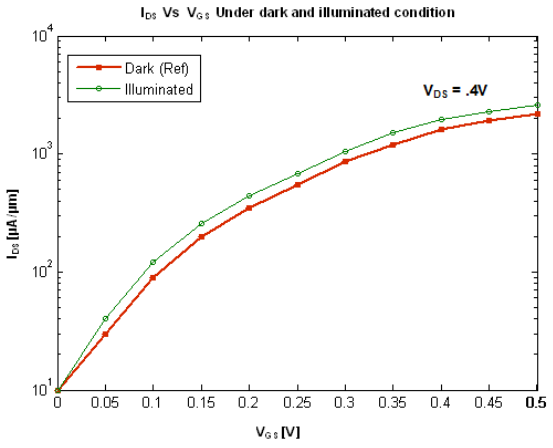

Fig. 6. Simulated I_{DS} versus V_{GS} Characteristics under dark and illuminated conditions for V_{DS} =0.4 V.

Next, we look at the full range I_{DS} *Vs* V_{GS} characteristics for the model device for a fixed value of V_{DS} = 0.4V as shown in Fig. 6. Current in the off-state (*VGS* = 0*; VDS* =0.4*V*), is comprised of two components; source-to-channel tunneling, for longitudinal energies below the source-to-channel barrier, and diffusion, for energies above the barrier. Therefore, the tunneling current component is increased in the off-state as a result of scattering. It is also found that the drain current under illuminated condition is more than under dark condition due to generation of excess carriers under illumination.

The ballistic current is a product of the charge density and the carrier velocity. The charge density within a device is primarily prescribed by 2D electrostatics and the velocity (for a given charge density) by the band structure. Therefore the effects of 2D electrostatics and band structure on device performance can be explained by examining the charge density and carrier velocity at a point within the device.

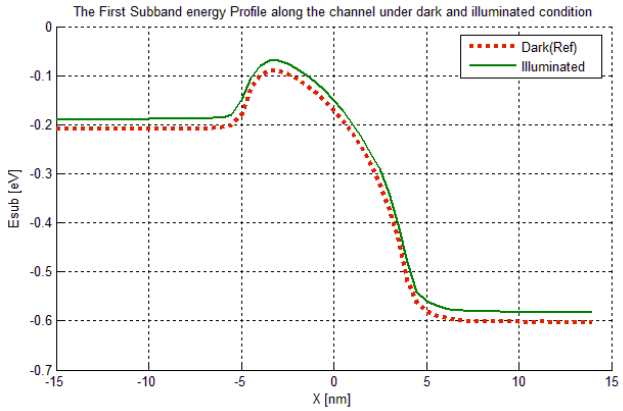

Fig. 7. Simulated first sub-band energy profile characteristics along the channel of the model DG SOI n-MOSFET under dark and illuminated conditionsat VGS = VDS = 0.6 V.

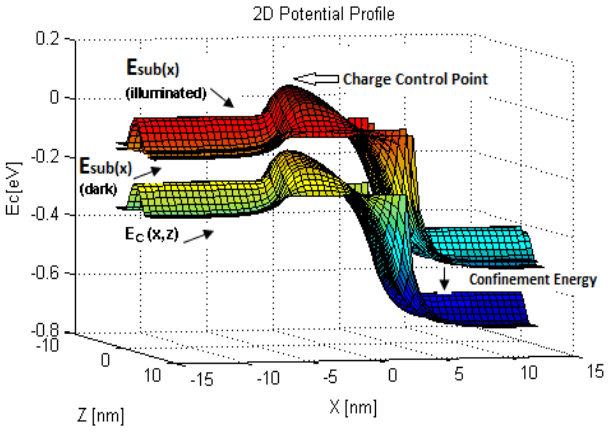

Fig. 8. Simulated 2-D conduction band edge profile and first sub-band energy profiles within the x-z cross section of the model DG SOI n-MOSFET under dark and illuminated conditions at VGS= VDS =0.6V.

We examine these quantities at the charge control point. To illustrate the charge control point, we plot the 2D potential and sub-band profiles(dark and illuminated) in the on-state (Fig. 8). Although the potential profile is a 2D function (*x* and *z* dimensions), the sub-bands are a function of *x* alone and represent the effective potential energy of the confined 2D carriers. The sub-band profiles exhibit a maximum as one move from the source to the drain. This point is referred to as the charge control point because it is a point where there is no carrier reflection due to the potential profile. Note that due to the thin nature of the body the n-MOSFET exhibits single sub-band occupancy. Note that the sub-band profile under illuminated condition exhibits a maximum charge control point than sub-band profile under dark condition due to the generation of extra carriers due to illumination.

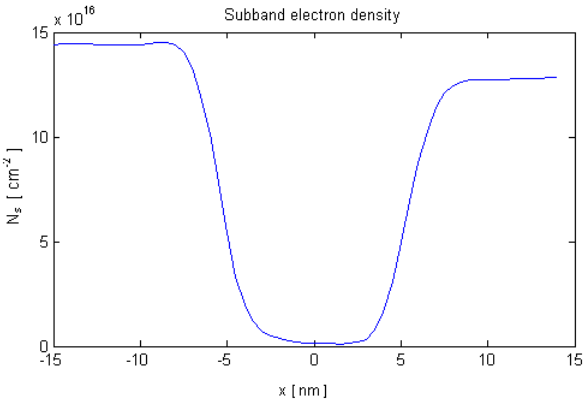

Fig. 9. Simulated 2-D electron density distributions along the channel along the length of the channel of the model DG SOI n-MOSFET under dark and illuminated conditions atVGS = VDS = 0.6 V.

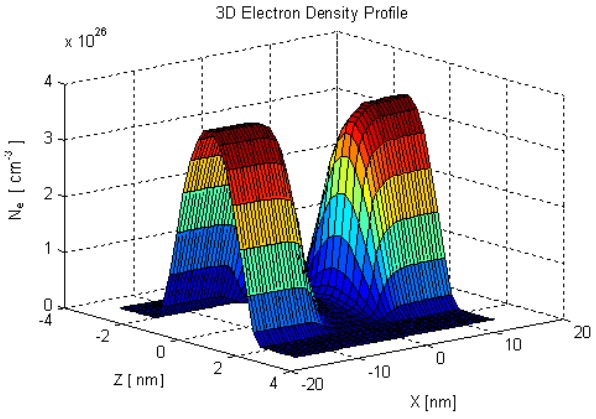

Fig. 10. Simulated 3-D electron density distributions within the x-z cross section of the model DG SOI n-MOSFET under dark and illuminated conditions at VGS = VDS = 0.6 V.

Figs. 8, 9 and 10 show the potential energy profiles and electron density in the x-z cross-section of the model DG SOI n-MOSFET as simulated with *VGS* = *VDS* = 0.6 V. It is observed that, the electron density reduces to zero

at the oxide/silicon interfaces due to well-known quantum effects. It is also observed that, there is a barrier region near the source end of the channel. This barrier determines the amount of electrons entering the channel. Its height is modulated by the gate bias.

5. Conclusion

The self-consistent 2-D numerical model presented in this paper can be used for the practical characterization of two dimensional nano-scale Double-Gate SOI n-MOSFET under illuminated condition for photodetection application. The quantum model using mode space approach based on the self-consistent solution of 2-D Poisson-Schrödinger equation has been obtained. Device characteristics like current-voltage characteristics, conduction band vs sub-band energy profile and sub-band electron density under dark and illuminated condition have been numerically estimated. Accurate results have been obtained with significantly reduced computational time.The accuracy of the model has been verified by comparing the results with that calculated by nanomos 2.5 device simulator. It is seen that the device has all qualities to be used as a photo detector in OEIC receivers. The present work is confined to modeling and simulation of uniformly doped two dimensional Double-Gate SOI n-MOSFET photodetectors. The future work can be carried out with three dimensional uniform doping and also with non-uniform doping. The detailed noise analysis can also be carried out to develop an equivalent circuit model for the accurate characteristics of the device for the use in OEIC applications.

References

[1] P. Chakrabarti, S. Kumar, P. K. Rout, B. G. Rappai, Proc.3rd Asia PacificMicrowave Conference, Tokyo, Japan, 1990, p. 575.

[2] P. Chakrabarti, I. Venugopal, Phys. Stat. Sol. (A), **128**, 521(1991).

[3] P. Chakrabarti, M. Madheswaran, A. Gupta, N. A. Khan, V. Rajamani, IETE Journal of Research, **46**, 205 (2000).

[4] P. Chakrabarti, B. K. Mishra, Y. Pratap Reddy, S. Prakash, Phys. Stat. Sol. (A), **147**, 277 (1995).

[5] K. Okamoto, S. Inoue, Solid-state Electronics, **16**, 657 (1973).

[6] M. Kabeer, K. Gowri, V. Rajamani, J. Optoelectron. Adv. Mater. **9**(9), 2879 (2007).

[7] International Technology Roadmap for Semiconductors 2009, Semiconductor Industry Association, San Jose, USA, Available from <http://public.itrs.net>.

[8] Y. Taur, L. H. Wann, D. J. Frank, IEDM Tech. Dig., 789 (1998).

[9] Y. Taur, D. A. Buchanan, W. Chen, D. J. Frank, K. E. Ismail, S.-H. Lo, G. A. Sai-Halasz, R. G. Viswanathan, H.-J. C. Wann, S. J. Wind, H.-S. P. Wong, Proc. IEEE, **85**(4), 486(1997).

[10] D. J. Frank, R. H. Dennard, E. Nowak, Proc. IEEE, **89**(3), 259 (2001).

[11] Y. Taur, Proc. Symp. VLSI Technology, 6 (1999).

[12] D. J. Frank, S. E. Laux, M. V. Fischetti, IEDM Tech. Dig., 553 (1992).

[13] D. J. Frank, S. E. Laux, M. V. Fischetti, IEEE Trans. Electron Devices, **40**, 2103 (1993).

[14] R.-H. Yan, A. Ourmazd, K. F. Lee, IEEE Trans. Electron Devices, **39**, 1704 (1992).

[15] Suzuki, K., T. Tanaka, Y. Tasaka, H. Horie, Y. Arimato, IEEE Trans.Electron Devices, **40**, 2326 (1993).

[16] J.-P. Colinge, Solid StateElectron., **48**(6), 897 (2004).

[17] H. K. Lim, J. G. Fossum, IEEE Transactions on electron devices, **30**, (1983).

[18] K. K. Young, IEEE Trans. Electron Devices, **36**(2), 399 (1989).

[19] Jason C. S. Woo, Kyle W. Terrill, Prahalad K. Vasudev, IEEE Transactions on Electron Devices **37**(9), (1990).

[20] Mishel Matloubian, Cheng-Eng Daniel Chen, Bor-Yen Mao, Ravishankar Sundaresan, Gordon P. Pollack, IEEE Transactions on Electron Devices, **37**(9), (1990).

[21] C. Mallikarjun, K. N. Bhat, IEEE Transactions on Electron Devices **37**(9), (1990).

[22] J.-Y. Guo, C.-Y. Wu, IEEE Trans. Electron Devices, **40**(9), 1653 (1993).

[23] Hans van Meer, Kristin De Meyer, IEEE Transactions on Electron Devices, **48**(10), (2001).

[24] Y. S. Pang, et. al, IEEE Trans. Electron Devices, **49**(12), 2209 (2002).

[25] M. Jagadesh Kumar, Anurag Chaudhry, IEEE Trans. Electron Devices, **51**(4), (2004).

[26] Elvis C. Sun, James B. Kuo, IEEE Trans. Electron Devices, **51**(4), (2004).

[27] Guruprasad Katti, itaDasGupta, Amitava Das Gupta, IEEE Transactions on Electron Devices, **51**(7). (2004).

[28] J. Yin, X. Shi, R. Huang, Solid State Electron., **50**, 1551 (2006).

[29] M. Miura-Mattauschet. al, IEEE Trans. Electron Devices, **53**(9), 1994 (2006).

[30] R. Rao, G. Katti, D. S. Havaldar, N. Dasgupta, A. Dasgupta, Solid State Electron., **53**(3), 256 (2009).

[31] Rathnamala Rao, Nandita Das Gupta, Amitava Das Gupta, IEEE Transactions on Device and materials reliability, **10**(2), (2010).

[32] F. Stern, J. Comput. Phys., **6**, 56 (1970).

[33] T. Kerkhoven, A. T. Galick, U. Ravaioli, J. H. Arends, Y. Saad, J. Appl. Phys., **68**, 3461 (1990).

[34] A. Trellakis, A. T. Galick, A. Pacelli, U. Ravaioli, J. Appl. Phys., **81**, 7880 (1997).

[35] H. R. Khan, D. Mamaluy, D. Vasileka, Institute of Physics Publishing, **107**, 01 (2007).

[36] G. Curatola, G. Iannaccone, Comput. Mater. Sci., **28**, 342 (2003).

[37] H. R. Khan, Mamaluy D., Vasileka D., IEEE Trans. Electron Devices, **54**, 784 (2007).
[38] G. Fiori, Iannaccone G., IEEE Trans. Nanotechnol., **6**, 524 (2007).
[39] J. B. Roldan, A. Godoy, F. Gamiz, M. Balaguer, IEEE Trans. Electron Devices, **55**, 411(2008).
[40] A. Rahman, J. Guo, S. Datta, M. S. Lundstrom, IEEE Trans. Electron Devices, **50**(9), 1853 (2003).
[41] R Venugopal, Z. Ren, S. Datta, M. S. Lundstrom, J. Appl. Phys., **92**, 373 (2002).
[42] Z. Ren, R. Venugopal, S. Goasguen, S. Datta, M. S. Lundstrom, IEEE Trans. Electron Devices, **50**, 1914 (2003).
[43] J. S. Blakemore, Solid state Electron, **25**, 1067 (1982).
[44] Zhibin Ren, MOSFETs: Physics, Simulation, and Design. Ph.D. Dissertation,Purdue University, West Lafatette, IN, (2001).

*Corresponding author: kabeer786india@gmail.com